Journal of the Mechanics and Physics of Solids 92 (2016) 127–136

Contents lists available at ScienceDirect

Journal of the Mechanics and Physics of Solids

journal homepage: www.elsevier.com/locate/jmps

Universality of the frequency spectrum of laminates

Gal Shmuel [a,*], Ram Band [b]

[a] Faculty of Mechanical Engineering, Technion–Israel Institute of Technology, Haifa 32000, Israel
[b] Department of Mathematics, Technion–Israel Institute of Technology, Haifa 32000, Israel

ARTICLE INFO

Article history:
Received 25 February 2016
Received in revised form
3 April 2016
Accepted 3 April 2016
Available online 7 April 2016

Keywords:
Laminate
Bloch–Floquet waves
Dispersion relation
Band-gap
Phononic crystal
Wave propagation
Frequency spectrum
Finite deformations

ABSTRACT

We show that the frequency spectrum of two-component elastic laminates admits a universal structure, independent of the geometry of the periodic-cell and the specific physical properties. The compactness of the structure enables us to rigorously derive the maximal width, the expected width, and the density of the *band-gaps* – ranges of frequencies at which waves cannot propagate. In particular, we find that the density of these band-gaps is a universal property of classes of laminates. Rules for tailoring laminates according to desired spectrum properties thereby follow. We show that the frequency spectrum of various finitely deformed laminates are also endowed with the same compact structure. Finally, we explain how our results generalize for laminates with an arbitrary number of components, based on the form of their dispersion relation.

1. Introduction

Wave propagation in heterogeneous media has fascinated the scientific community for decades. The inhomogeneity causes multiple scattering, and, in turn, wave interferences that give rise to intriguing phenomena in various fields. Of particular interest are the transition of conducting to isolating behavior of electronic crystals, localization of electromagnetic waves in dielectrics (Yablonovitch, 1993), and attenuation of mechanical motions in elastic media (Kushwaha et al., 1993; Ruzzene and Baz, 1999; Garcia-Pablos et al., 2000; Henderson et al., 2001; Kim and Yang, 2014). The significance of the latter stems from its central role in numerous applications; transducers (Smith and Auld, 1991), waveguides (Miyashita, 2005), vibration filters (Khelif et al., 2003), acoustic imaging for medical ultrasound and nondestructive testing (Olsson III and El-Kady, 2009), noise reduction (Elser et al., 2006) and cloaking (Milton et al., 2006; Colquitt et al., 2014) are just a few examples. The mathematical and physical richness of elastic waves in heterogeneous materials emanates from their vectorial nature, and their spatial dependency on additional constituents parameters.

Layered media have been extensively studied (Adams et al., 2008; Willis, 2009; Gomopoulos et al., 2010; Psarobas et al., 2010; Walker et al., 2010; Nemat-Nasser and Srivastava, 2011; Schneider et al., 2012, 2013; Rudykh and Boyce, 2014), on account of their relative simplicity of fabrication and theoretical modeling. This work provides new insights on the relation between their geometry, physical properties, and frequency spectrum. First, we find a universal representation of the spectrum, *independent* of the unit-cell geometry and specific constituents properties. This representation is defined on a compact object, which enables us to rigorously derive the maximal width, the expected width, and the density of the

* Corresponding author.
E-mail address: meshmuel@tx.technion.ac.il (G. Shmuel).

http://dx.doi.org/10.1016/j.jmps.2016.04.001
0022-5096/

band-gaps – ranges of frequencies at which waves cannot propagate. In particular, we find that the gap-density is a universal property, namely, it is invariant under the change of the geometry of the periodic-cell, and certain changes in the constituents mechanical properties. The spectral characteristics determined are identified with classes of compositions, hence provide rules for tailoring the laminate according to desired properties of the gaps. Thus far, such calculations would necessitate the truncation of infinite spectra, thereby leading to estimates rather than accurate results.

The canvas upon which the analysis is presented is of two-component elastic laminates, also termed one-dimensional phononic crystals. The conclusions we draw, however, extend to additional systems. By virtue of the similarity between electromagnetic and elastodynamics wave equations for the considered geometry, our insights apply to photonic crystals as well (Shmuel and Band, 2016). The spectrum of stratified piezoelectrics is also endowed with our compact representation, owing to a similar dispersion relation (Qian et al., 2004). In certain cases, our analysis further applies to laminates comprising soft non-linear materials. Such materials are capable of undergoing finite deformations, thereby their mechanical properties are changed, and their spectrum is rendered tunable. Our approach facilitates characterizing this tunability, as demonstrated in the forthcoming. We explain how our results generalize for laminates with an arbitrary number of components, based on the form of their dispersion relation.

This paper is composed as follows. Section 2 derives the equation governing elastic wave propagation in two-component laminates. Section 3 introduces a universal structure for the spectrum of the laminates by means of a dynamic flow on a compact object. Using this structure, Section 4 analyzes spectral characteristics and provides optimization results of the band-gaps. The applicability of the analysis to particular cases of elastic waves in finitely deformed laminates is demonstrated in Section 5. The paper is concluded with a summary of our main results and our future objectives in Section 6.

2. Wave propagation in laminates

The formulation of elastic wave propagation in layered composites is found in various sources in the literature (*e.g.*, Ziegler, 1977); the standard approach is summarized here, for completeness.

Consider an infinite laminate made out of two alternating linearly elastic layers (Fig. 1a), repeating periodically in the direction $\mathbf{n}$. We denote the layers with 1 and 2, and their associated quantities with superscript (p), $p=1$ and 2, respectively. In the absence of body forces, Cauchy equations of motion governing the displacement field $\mathbf{u}^{(p)}(\mathbf{x}, t)$ in each layer read (see, for instance, Graff, 1975)

$$\left(\lambda^{(p)}+\mu^{(p)}\right)\nabla\nabla\cdot\mathbf{u}^{(p)}+\mu^{(p)}\nabla^2\mathbf{u}^{(p)}=\rho^{(p)}\ddot{\mathbf{u}}^{(p)}. \tag{1}$$

Herein, $\lambda^{(p)}$ and $\mu^{(p)}$ are the Lamé coefficients of each layer, where $\rho^{(p)}$ is the mass density. Time-harmonic plane waves propagating along the lamination direction are of the form

$$\mathbf{u}^{(p)}=\mathbf{m}^{(p)}e^{ik^{(p)}\left(\mathbf{n}\cdot\mathbf{x}-c^{(p)}t\right)}, \tag{2}$$

where $k^{(p)}$ and $c^{(p)}$ are the wavenumber and phase velocity in each layer, respectively. The frequency of the waves, ω, is thus $\omega=c^{(p)}k^{(p)}$. The relation between the phase velocity and the polarization of the waves, $\mathbf{m}^{(p)}$, is determined through substituting Eq. (2) into Eq. (1)

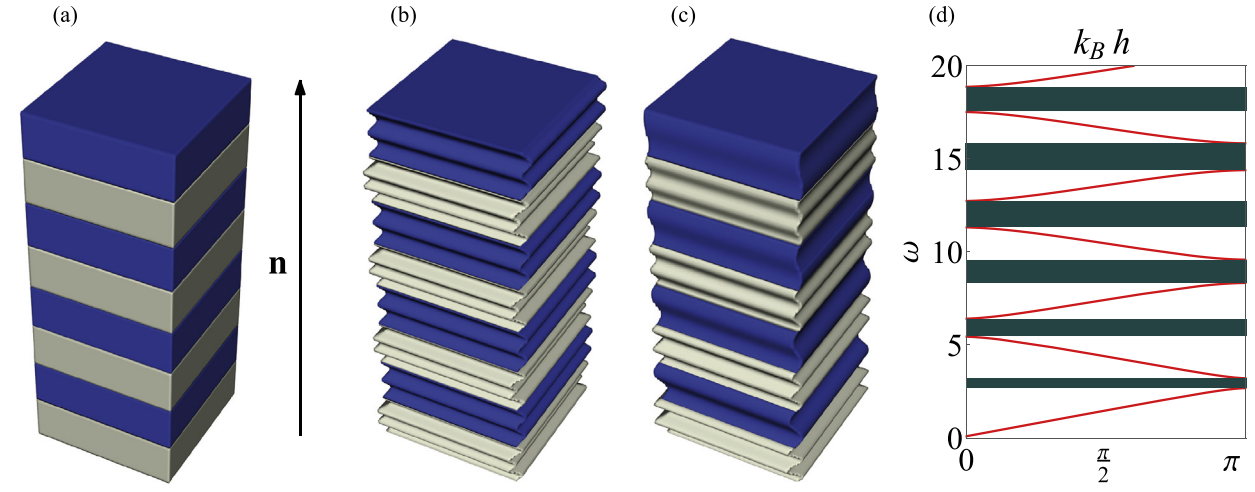

Fig. 1. (a) A laminate comprising two alternating layers, repeated periodically in direction $\mathbf{n}$. (b) Propagating waves, associated with frequencies for which $|\eta|<1$. (c) Attenuating waves, associated with frequencies for which $|\eta|>1$. (d) Representative band structure of an exemplary laminate. Colored regions denote band-gaps. (For interpretation of the references to color in this figure caption, the reader is referred to the web version of this paper.)

$$\left(\lambda^{(p)}+\mu^{(p)}\right)\left(\mathbf{m}^{(p)}\cdot\mathbf{n}\right)\mathbf{n}+\left(\mu^{(p)}-\rho^{(p)}c^{(p)^2}\right)\mathbf{m}^{(p)}=\mathbf{0}. \tag{3}$$

Eq. (3) implies that either $\mathbf{m}^{(p)}$ is perpendicular to $\mathbf{n}$, for which

$$c^{(p)}=\sqrt{\frac{\mu^{(p)}}{\rho^{(p)}}}=:c_T^{(p)}, \tag{4}$$

or that $\mathbf{m}^{(p)}$ is parallel to $\mathbf{n}$, and then

$$c^{(p)}=\sqrt{\frac{\lambda^{(p)}+2\mu^{(p)}}{\rho^{(p)}}}=:c_L^{(p)}. \tag{5}$$

At planes perpendicular to $\mathbf{n}$, the resulting traction is

$$\mathbf{t}^{(p)}=ik^{(p)}\tilde{\mu}^{(p)}\mathbf{m}^{(p)}e^{ik^{(p)}\left(\mathbf{n}\cdot\mathbf{x}-c^{(p)}t\right)}, \tag{6}$$

where $\tilde{\mu}^{(p)}=\mu^{(p)}$ for the former mode of *transverse* waves, and $\tilde{\mu}^{(p)}=\lambda^{(p)}+2\mu^{(p)}$ for the latter mode of *longitudinal* waves.

From Eqs. (2) and (6), the relation between the traction and the displacement at the boundaries of each layer is

$$\begin{pmatrix}\mathbf{u}^{(p)}(\mathbf{x}+h^{(p)}\mathbf{n})\\ \mathbf{t}^{(p)}(\mathbf{x}+h^{(p)}\mathbf{n})\end{pmatrix}=\begin{bmatrix}\cos k^{(p)}h^{(p)} & \dfrac{\sin k^{(p)}h^{(p)}}{\tilde{\mu}^{(p)}k^{(p)}}\\ -\tilde{\mu}^{(p)}k^{(p)}\sin k^{(p)}h^{(p)} & \cos k^{(p)}h^{(p)}\end{bmatrix}\begin{pmatrix}\mathbf{u}^{(p)}(\mathbf{x})\\ \mathbf{t}^{(p)}(\mathbf{x})\end{pmatrix}, \tag{7}$$

where $h^{(p)}$ is the thickness of layer p, and the time dependency were omitted, for brevity. The matrix in Eq. (7), which we denote by $\mathrm{T}^{(p)}$, is known as the layer *transfer* matrix. At the interfaces between the layers, the traction and the displacement fields must be continuous, therefore

$$\begin{pmatrix}\mathbf{u}^{(1)}(\mathbf{x}+h^{(p)}\mathbf{n})\\ \mathbf{t}^{(1)}(\mathbf{x}+h^{(p)}\mathbf{n})\end{pmatrix}=\begin{pmatrix}\mathbf{u}^{(2)}(\mathbf{x}+h^{(p)}\mathbf{n})\\ \mathbf{t}^{(2)}(\mathbf{x}+h^{(p)}\mathbf{n})\end{pmatrix}. \tag{8}$$

Applying Eq. (7) twice allows to relate the traction and the displacement fields at the boundaries of the repetitive cell, providing

$$\begin{pmatrix}\mathbf{u}^{(1)}(\mathbf{x}+h\mathbf{n})\\ \mathbf{t}^{(1)}(\mathbf{x}+h\mathbf{n})\end{pmatrix}=\mathrm{T}^{(2)}\mathrm{T}^{(1)}\begin{pmatrix}\mathbf{u}^{(1)}(\mathbf{x})\\ \mathbf{t}^{(1)}(\mathbf{x})\end{pmatrix}, \tag{9}$$

where $h=h^{(1)}+h^{(2)}$. In conjunction with Eq. (9), the fields at the boundaries are also related via the Bloch–Floquet condition, requiring them to be identical up to a phase shift, namely

$$\begin{pmatrix}\mathbf{u}^{(1)}(\mathbf{x}+h\mathbf{n})\\ \mathbf{t}^{(1)}(\mathbf{x}+h\mathbf{n})\end{pmatrix}=e^{ik_Bh}\begin{pmatrix}\mathbf{u}^{(1)}(\mathbf{x})\\ \mathbf{t}^{(1)}(\mathbf{x})\end{pmatrix}, \tag{10}$$

where k_B is called the Bloch wavenumber. Combining Eqs. (9) and (10) constitutes an eigenvalue problem, whose solution delivers the following *dispersion relation* (Rytov, 1956)

$$\eta=\cos k_Bh, \tag{11}$$

with

$$\eta=\cos\frac{\omega h^{(1)}}{c^{(1)}}\cos\frac{\omega h^{(2)}}{c^{(2)}}-\gamma\sin\frac{\omega h^{(1)}}{c^{(1)}}\sin\frac{\omega h^{(2)}}{c^{(2)}}, \tag{12}$$

where $\gamma=\frac{1}{2}\left(\frac{\rho^{(1)}c^{(1)}}{\rho^{(2)}c^{(2)}}+\frac{\rho^{(2)}c^{(2)}}{\rho^{(1)}c^{(1)}}\right)$ quantifies the contrast between the constituents impedance. Eq. (11) governs the motion of the laminate, by relating the velocity, the length, and the frequency of the Bloch-waves. The frequency spectrum is obtained by solving Eq. (11) for values of k_B in the irreducible 1st Brillouin zone $0\le k_Bh\le\pi$ (Farzbod and Leamy, 2011). Waves propagate without attenuation when $|\eta|<1$ (Fig. 1b). Conversely, band-gaps correspond to ranges of frequencies of evanescent waves, for which $|\eta|>1$ (Fig. 1c). A representative band structure of an exemplary laminate is illustrated in Fig. 1d, where the colored regions denote the band-gaps. Notwithstanding numerous analyses of Eq. (11), new insights about the spectrum are found, owing to the following new approach.

3. A universal spectrum structure

Our analysis of the spectrum benefits from a technique developed for the study of Schrödinger operators on metric graphs (Barra and Gaspard, 2000; Berkolaiko and Winn, 2010; Band and Berkolaiko, 2013). The system we consider

necessitates a suitable variation of that approach, as follows. Upon defining the variables

$$\zeta^{(p)} := \frac{\omega h^{(p)}}{c^{(p)}}, \tag{13}$$

one can write η as a function of γ, $\zeta^{(1)}$ and $\zeta^{(2)}$, namely

$$\eta\left(\zeta^{(1)}, \zeta^{(2)}; \gamma\right) := \cos\zeta^{(1)} \cos\zeta^{(2)} - \gamma \sin\zeta^{(1)} \sin\zeta^{(2)}. \tag{14}$$

Fixing γ, we observe that η is a 2π-periodic function of $\zeta^{(1)}$ and $\zeta^{(2)}$. Therefore, we can consider η as a function on a torus of edge length 2π, whose coordinates are $(\zeta^{(1)}, \zeta^{(2)})$. We note that this function is *independent* of the thickness of the layers and their specific physical properties. For illustration, contours of representative level sets of η in the range $|\eta| < 1$ are plotted in Fig. 2a, at $\gamma = 5$, where each curve corresponds to a real value of k_B. Whether k_B is real and corresponds to a pass-band, or imaginary and corresponds to a band-gap, depends purely on the absolute value $|\eta|$. Eq. (12) shows that this absolute value $|\eta(\zeta^{(1)}, \zeta^{(2)})|$ is invariant under the transformations $\zeta^{(p)} \to \zeta^{(p)} + \pi$. Hence, we exploit this symmetry to make a further reduction, and fold the torus into a π-periodic torus. We denote the new torus by $\mathbb{T}$, and denote by $\mathbb{D}$ its subdomain where $|\eta(\zeta^{(1)}, \zeta^{(2)})| > 1$, *i.e.*, where Eq. (11) is satisfied with imaginary k_B. Fig. 2b shows this torus as a square whose opposite edges are identified, and depicts representative domains of $\mathbb{D}$ which correspond to exemplary values of γ. Specifically, the gray, blue, and orange regions correspond to $\gamma = 2$, 5 and 10, respectively. The boundary of $\mathbb{D}$ consists of a lower curve and an upper curve, which we denote by C_l and C_u, respectively. On these curves $\eta = -1$. To show that, we get from Eq. (14)

$$\eta\left(\zeta^{(1)}, \zeta^{(2)}; \gamma\right) = \cos\zeta^{(1)} \cos\zeta^{(2)} - \gamma \sin\zeta^{(1)} \sin\zeta^{(2)} \le \cos\zeta^{(1)} \cos\zeta^{(2)} - \sin\zeta^{(1)} \sin\zeta^{(2)} = \cos\left(\zeta^{(1)} + \zeta^{(2)}\right) \le 1, \tag{15}$$

bearing in mind that $(\zeta^{(1)}, \zeta^{(2)}) \in [0, \pi)^2$ on $\mathbb{T}$ and $\gamma \ge 1$. By definition, $|\eta| > 1$ on $\mathbb{D}$ and this combined with the last inequality implies that $\eta < -1$ on $\mathbb{D}$. From the continuity of η we deduce that indeed $\eta = -1$ on C_l and C_u. Plugging this value into Eq. (14) provides the following expressions for the curves:

$$\zeta^{(2)} = \pi - \arccos\left[\frac{\cos\zeta^{(1)} \pm \gamma\sqrt{\gamma^2 - 1}\,\sin^2\zeta^{(1)}}{1 + \left(\gamma^2 - 1\right)\sin^2\zeta^{(1)}}\right], \tag{16}$$

where the upper (resp. lower) curve C_u (resp. C_l) corresponds to the plus (resp. minus) sign in the numerator. The function η on $\mathbb{T}$ is invariant under π-rotation of $\mathbb{T}$ around its middle, given by the transformation $(\zeta^{(1)}, \zeta^{(2)}) \to (\pi - \zeta^{(1)}, \pi - \zeta^{(2)})$, and under reflection across the line $\zeta^{(2)} = \pi - \zeta^{(1)}$, by the transformation $(\zeta^{(1)}, \zeta^{(2)}) \to (\pi - \zeta^{(2)}, \pi - \zeta^{(1)})$. Each of those transformations leaves the domain $\mathbb{D}$ invariant and exchanges between its boundary curves C_l and C_u.

The torus structure is endowed with a dynamic flow $\vec{\zeta}(\omega)$ which characterizes the spectrum, when Eq. (13) is interpreted as

$$\vec{\zeta}\left(\omega\right) = \omega \cdot \left(\frac{h^{(1)}}{c^{(1)}}, \frac{h^{(2)}}{c^{(2)}}\right) \bmod \pi. \tag{17}$$

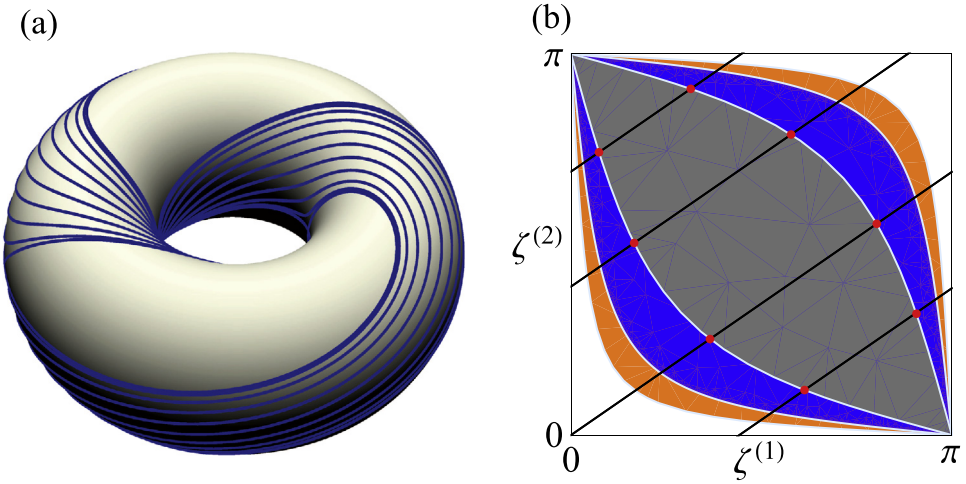

Fig. 2. (a) Representative contours on the torus at which $\left|\eta(\zeta^{(1)}, \zeta^{(2)})\right| < 1$, when $\gamma = 5$. Each curve is identified with a real value of k_B. (b) Representative domains of $\mathbb{D}$ over the square-identification of the folded torus. Gray, blue, and orange regions correspond to $\gamma = 2$, 5 and 10, respectively. Red dots designate the intersections of the flow with the boundary of $\mathbb{D}$, when $\gamma = 2$. (For interpretation of the references to color in this figure caption, the reader is referred to the web version of this paper.)

The frequency ω has the role of a time-like parameter. Band-gaps are identified with values of ω for which the flow $\vec{\zeta}(\omega)$ coincides with $\mathbb{D}$. For illustration, the diagonal lines in Fig. 2b represent a part of an exemplary flow; its intersections with the boundary of $\mathbb{D}$ at $\gamma=2$ are marked with red dots. The direction of the flow on the torus is given by the ratio

$$a_f = \frac{h^{(2)}}{h^{(1)}}\frac{c^{(1)}}{c^{(2)}}. \tag{18}$$

For the generic case of an irrational ratio, the flow covers the torus ergodically, with a uniform measure (Katok and Hasselblatt, 1996), as illustrated in the supplementary data available online. Using the ergodicity of the flow, we may *replace spectral averages by averaging over a compact object*, namely, the torus.

4. Analysis on the torus

The first question we address is: What is the probability that a randomly chosen frequency is within a band-gap? A determination of the probability requires the calculation of the relative sizes of the band-gaps and the pass-bands. In the frequency domain, it is a difficult task, perhaps impossible, to determine how this *gap-density* converges as the frequency interval approaches infinity. However, over the compact torus, *the density of the gaps is merely the relative area of* $\mathbb{D}$ *in* $\mathbb{T}$; its calculation is a simple integral of the *closed-form* expression

$$1 - \frac{2}{\pi^2}\int_0^{\pi} C_l \, \mathrm{d}\zeta^{(1)}. \tag{19}$$

We arrive at a counter-intuitive and peculiar result – at a prescribed γ, the gap-density is completely *independent* of the volume fractions of the layers. To illustrate this statement, consider the following example. Compose a laminate of equal volume fractions of materials (1) and (2). Compose a second laminate by introducing an *infinitesimal* amount of (1) into a bulk of (2). The probability that an arbitrary frequency pertains to a band-gap is *identical* in the two laminates.

We demonstrate the calculation of the gap-density, with the following example. We evaluate numerically the dispersion relation in Eq. (11) over increasing segments of frequencies; at each segment, we calculate the ratio between the total length of its band-gaps and the segment length; we carry out the calculation for four elastic laminates, which differ by the layers properties and volume fractions. The mass densities, shear moduli and thicknesses of layer (1) are specified in Table 1. The properties of layer (2) are fixed at $\rho^{(2)} = 1000$ kg/m^3 and $\mu^{(2)} = 200$ kPa, where $h^{(2)}$ is chosen such that $h^{(1)} + h^{(2)} = 1$ mm. The calculation is illustrated in Fig. 3a. Therein, the gray curve with circle marks, red curve with star marks, green curve with triangle marks, and the blue curve with diamond marks correspond to layer (1) properties in columns *a*, *b*, *c* and *d* of Table 1, respectively. We observe the convergence of these curves to the ratio between the subdomain and area of the torus, calculated via Eq. (19) and denoted by the black dashed line. Examination of the flow on the torus reveals that the rate of convergence becomes slower as a_f approaches a rational number, zero, or infinity. In the limit of these cases the flow covers only a one-dimensional subspace of $\mathbb{T}$, which depends on a_f. Once a_f slightly deviates from these cases, the flow would deviate from the corresponding one-dimensional subspace, and will eventually cover a dense subset of the torus. The closer the a_f is to these values, the slower the flow deviates and the slower the band-gap ratio converges. This is demonstrated by considering again a laminate whose layer (1) properties are given in column *d*. We compare the case when $h^{(1)} = 0.2$, $h^{(2)} = 0.8$, with the case $h^{(1)} = 0.01$, $h^{(2)} = 0.99$, denoted Fig. 3b by the blue curve with diamond marks, and the brown curve with asterisk marks, respectively. The physical properties of layer (2) are again $\rho^{(2)} = 1000$ kg/m^3 and $\mu^{(2)} = 200$ kPa.

The widths of the gaps are investigated next. We recognize that these widths, denoted by $\Delta\omega$, are related to lengths of intervals directed along the flow, denoted by $\Delta\zeta$, whose endpoints lie on C_u and C_l (see Fig. 2b), via

$$\Delta\omega = \frac{\kappa^{(1)}\kappa^{(2)}}{\sqrt{\left(\kappa^{(1)}\right)^2 + \left(\kappa^{(2)}\right)^2}}\Delta\zeta, \tag{20}$$

where

$$\kappa^{(p)} = c^{(p)}/h^{(p)}. \tag{21}$$

Table 1
Mass-densities, shear moduli and thicknesses of layer (1).

Material	*a*	*b*	*c*	*d*
ρ (kg/m^3)	2000	500	2000	500
μ (kPa)	7.18	28.7	1392	5571
h (mm)	0.8	0.6	0.4	0.2

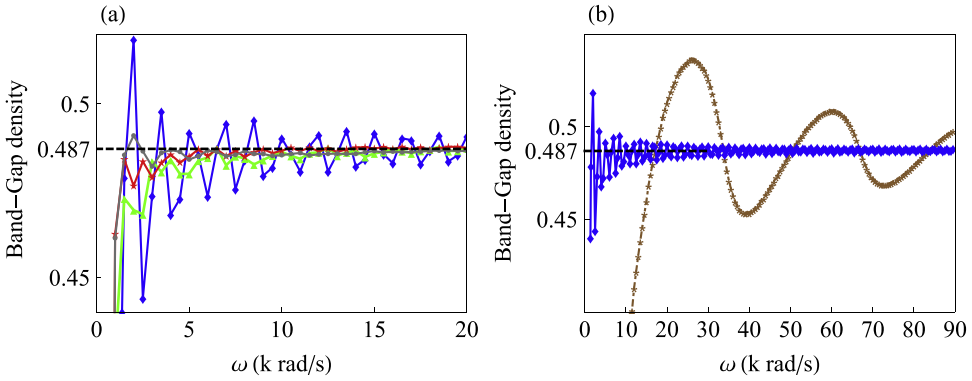

Fig. 3. (a) Numerical simulation of the gap-density convergence of four laminates. The gray curve with circle marks, red curve with star marks, green curve with triangle marks, and the blue curve with diamond marks, respectively, correspond to layer (1) whose properties are given in columns *a*, *b*, *c* and *d* in Table 1, respectively. The properties of layer (2) are $\rho^{(2)} = 1000$ kg/m^3 and $\mu^{(2)} = 200$ kPa, and $h^{(2)} = 1 - h^{(1)}$. The black dashed curve corresponds to the calculation of the ratio between the area of $\mathbb{D}$ and $\mathbb{T}$. (b) A comparison of the gap-density convergence of layer (1) whose properties are given in column *d*, when $h^{(1)} = 0.2$ mm and $h^{(1)} = 0.01$ mm, denoted by the blue curve with diamond marks, and the brown curve with asterisk marks, respectively. The properties of layer (2) are the same as in Fig. 3a. (For interpretation of the references to color in this figure caption, the reader is referred to the web version of this paper.)

We associate each length $\Delta\zeta$ with the parameters a_f and b_f which characterize the line equation of its corresponding flow interval

$$\zeta^{(2)} = a_f \zeta^{(1)} + b_f, \tag{22}$$

with $a_f \in [0, \infty)$, $b_f \in [-\pi a_f, \pi]$. These observations, together with the derived expressions for the curves C_u and C_l, enable determining the width of the gaps, and relating it to the physical and geometrical properties of the laminate. As the whole spectrum is encapsulated in the torus, we are able, in turn, to formulate optimization problems rigorously.

We start with the 1st gap, whose width maximization is of practical importance, being the one which is most often realized experimentally (Gomopoulos et al., 2010; Schneider et al., 2012, 2013). We would like to know: given two materials, what is the microstructure which maximizes the 1st gap? The 1st gap is identified with the flow line emanating from the origin. Therefore, we seek the slope a_f which maximizes the right-hand side of Eq. (20), at $b_f = 0$. The problem is interpreted as a search for an optimal $h^{(2)}/h^{(1)}$ at fixed $c^{(p)}$.

To that end, the calculation over the torus serves as an alternative to a calculation of the 1st gap-width for all possible compositions, via a partial spectra evaluation. Calculations over the torus become a *necessity* when the whole spectrum needs to be analyzed. Without proving that the spectrum can be encapsulated in the torus, there is not any way to know if calculations over a necessarily truncated subdomain of an infinite frequency domain are indeed close to the limit. This is the case for the gap-density, as for what follows, starting with the greatest gap width. We address two different practical scenarios. The first scenario considers a given laminate, with prescribed geometrical and physical properties. The objective is delivered by finding the maximal $\Delta\zeta$ within the segments along flows of the prescribed slope a_f, *i.e.*, maximizing over translations b_f, and plugging it into Eq. (20). We emphasize that this optimization is defined solely over $\mathbb{D}$, in an exact manner. Contrarily, a direct approach will require the evaluation of an infinite spectrum; since in practice it must be truncated, such approach provides only an approximation. The second scenario we consider is of a laminate with prescribed constituents, before choosing their volume fractions. In this case, the maximal gap is obtained by maximizing the right-hand side of Eq. (20), over all slopes a_f and translations b_f.

We supplement the discussion regarding optimality noting that our approach allows for quick calculation of bounds on the gaps-width, based on bounding $\Delta\zeta$. We find that for $\gamma < \gamma_{cr}$, where $\gamma_{cr} \approx 5.45$, the maximal $\Delta\zeta$, denoted $\Delta\zeta_{\max}$, is obtained at the intersection of $\mathbb{D}$ with $\zeta^{(1)} = \pi/2$. Utilizing Eq. (16), it is expressed in closed-form as

$$\Delta\zeta_{\max} = \pi - 2\arccos\left(\frac{\sqrt{\gamma^2 - 1}}{\gamma}\right). \tag{23}$$

Eq. (20) yields the following upper bound on the band-gap width:

$$\Delta\omega < \frac{\kappa^{(1)}\kappa^{(2)}}{\sqrt{{\kappa^{(1)}}^2 + {\kappa^{(2)}}^2}}\Delta\zeta_{\max}, \tag{24}$$

from which the following two quick bounds are obtained:

$$\Delta\omega < \frac{\max\left(\kappa^{(1)}, \kappa^{(2)}\right)}{\sqrt{2}}\Delta\zeta_{\max} \quad \text{and} \quad \Delta\omega < \min\left(\kappa^{(1)}, \kappa^{(2)}\right)\Delta\zeta_{\max}. \tag{25}$$

When $\gamma > \gamma_{cr}$, associated with large impedance contrasts, $\Delta\zeta_{max}$ is attained along the diagonal, for which $\zeta^{(1)} = \zeta^{(2)}$. The corresponding value for $\Delta\zeta_{max}$ is more cumbersome than the one in (23) and we do not specify it here. Yet, the bounds (24)–(25) apply in this case as well, once the corresponding value of $\Delta\zeta_{max}$ is plugged in. We note that for $\gamma < \gamma_{cr}$, the bound on the gap width is obtained as a limiting case of $\kappa^{(p)} \to \infty$ for $p=1$ or 2. For $\gamma > \gamma_{cr}$, the bound is actually realizable as a maximal gap width of laminate with $\kappa^{(1)} = \kappa^{(2)}$. Eqs. (24)–(25) provide explicit expressions for the maximal gap width in terms of the laminate properties. To the best of our knowledge, such bounds were not accessible so far.

The analysis is concluded with expressions for statistical characteristics of the spectrum, evaluated exactly using our representation. Specifically, the expected value of the gap-width of a prescribed system is determined via

$$\frac{\kappa^{(1)}}{\sqrt{1+a_f^2}}\mathrm{E}, \tag{26}$$

and the variance is calculated by

$$\frac{{\kappa^{(1)}}^2}{\pi\left(1+a_f\right)\left(1+a_f^2\right)}\int_{b_f=-a_f\pi}^{b_f=\pi}\left[\Delta\zeta\left(b_f\right)-\mathrm{E}\right]^2\mathrm{d}b_f, \tag{27}$$

with $\mathrm{E}=\frac{1}{\pi(1+a_f)}\int_{b_f=-a_f\pi}^{b_f=\pi}\Delta\zeta(b_f)\mathrm{d}b_f$ and $a_f=\kappa^{(1)}/\kappa^{(2)}$. We emphasize again that deriving these results using a direct approach involves calculations over truncations of an infinite spectrum, thereby leading to estimates rather than rigorous results.

5. Waves superposed on finite deformations

Soft materials capable of sustaining large strains attract a growing interest by virtue of the ability to control their functionalities via deformations (Mullin et al., 2007; Wang et al., 2014; Robertson et al., 2015). Interestingly, in certain setting, our analysis applies to laminates whose layers are made out of such constituents (deBotton, 2005; Rudykh and Boyce, 2014). Specifically, as shown in the sequel, the dispersion relation of small-amplitude waves superposed on certain large deformations is endowed with the torus representation. The resultant strains affect the dispersion relation, and thus render the spectrum tunable. In addition to the applicability of all the results mentioned in previous sections, our representation further provides a convenient tool for characterizing this tunability. This is demonstrated by way of example, using the theory of incremental dynamics of pre-deformed elastic materials. The formulation is given concisely, as our focus is on the dispersion relation; a comprehensive description of the theory is found, *e.g.*, in Ogden (1997) and Destrade and Saccomandi (2007).

Consider an infinite laminate made out of alternating layers of two soft materials. The laminate is subjected to a prescribed force in the lamination direction, and is free of mechanical loading in the perpendicular directions. We introduce a Cartesian system in which x_1 is along the lamination direction. In these coordinates, the resulting piecewise-homogeneous deformation is compatible with the following representation of its gradient, $\mathbf{F}$, in each layer:

$$\left[\mathrm{F}\right]^{(p)}=\mathrm{diag}\left[\lambda_1^{(p)},\lambda_2^{(p)},\lambda_3^{(p)}\right]. \tag{28}$$

$\mathbf{F}$ transforms line elements between the initial and deformed configurations. Accordingly, the *stretch ratio* $\lambda_1^{(p)}$ relates the resultant thickness of each layer, *i.e.*, $h^{(p)}$, to the thickness before the deformation, say $H^{(p)}$, via $h^{(p)}=\lambda_1^{(p)}H^{(p)}$. Assuming a perfect bonding between the layers, the stretch ratios in the plane of the layers are identical, namely

$$\lambda_2^{(1)}=\lambda_2^{(2)}=:\lambda_2,\quad \lambda_3^{(1)}=\lambda_3^{(2)}=:\lambda_3. \tag{29}$$

Once the constitutive behavior of the constituents is specified in terms of a *strain-energy function* $\Psi(\mathbf{F})$, one can determine the stretch ratios as follows. The stretches $\lambda_1^{(1)}$ and $\lambda_1^{(2)}$ are related via the continuity of the traction across the interface between the layers. In turn, these stretches are connected to the prescribed force by the requirement that its area density equals the traction on that surface. The remaining stretches are determined via the force-free boundary conditions at the perpendicular directions. Therefore, we treat the stretches henceforth as known quantities.

On top of the deformed configuration, we consider an incremental time-dependent displacement field $\mathbf{u}(\mathbf{x},t)$. We write the equations governing for the the field in each layer $\mathbf{u}^{(p)}(\mathbf{x},t)$ in the form

$$\nabla\cdot\left(\boldsymbol{C}^{(p)}\nabla\mathbf{u}^{(p)}\right)=\rho^{(p)}\ddot{\mathbf{u}}^{(p)}, \tag{30}$$

where, in components, $\boldsymbol{C}^{(p)}$ is

$$C_{ijkl}^{(p)}=\frac{1}{\det\mathbf{F}^{(p)}}F_{j\alpha}^{(p)}\frac{\partial^2\Psi^{(p)}}{\partial F_{i\alpha}\partial F_{k\beta}}F_{l\beta}^{(p)}. \tag{31}$$

The current mass-density is related to the initial density ρ_0 via $\rho=\rho_0/\det\mathbf{F}$. For simplicity, we focus on transverse motions, where a similar derivation is feasible for longitudinal motions. Accordingly, $\mathbf{u}(\mathbf{x},t)=u_2(x_1,t)\mathbf{j}$, where $\mathbf{j}$ is a unit-vector along

x_2, and Eq. (30) reduces to

$$C^{(p)}_{2121}u^{(p)}_{2,11} = \rho^{(p)}\ddot{u}^{(p)}_2. \tag{32}$$

Eq. (32) implies that the phase velocity equals

$$c^{(p)} = \sqrt{C^{(p)}_{2121}/\rho^{(p)}}, \tag{33}$$

hence depends on the underlying deformation and the constitutive law of the layer. One can now follow precisely the same scheme described in Section 2 to derive the dispersion relation, and recover Eq. (11). However, the physical and geometrical quantities therein are now functions of the finite deformation, and hence render the spectrum tunable. The effect of this dependency is explored next, when considering specific constitutive relations, using our compact representation. While we use *Neo-Hookean* and *Gentian* energy functions, the applicability of our representation is independent of the form of $\Psi^{(p)}(\mathbf{F})$, and relies only on the fact that the bias fields are piecewise-constant.

Neo-Hookean layers are governed by the energy

$$\Psi^{(p)}\left(\mathbf{F}\right) = \frac{\mu^{(p)}}{2}\left(\operatorname{tr}\mathbf{F}^{\mathrm{T}}\mathbf{F} - 3\right) - \mu^{(p)}\ln\det\mathbf{F} + \frac{\lambda^{(p)}}{2}(\ln\det\mathbf{F})^2, \tag{34}$$

for which

$$C^{(p)}_{2121} = \frac{{\lambda^{(p)}_1}^2\mu^{(p)}}{\lambda^{(p)}_1\lambda_2\lambda_3}. \tag{35}$$

A simple calculation shows that $\kappa^{(p)}$ and the flow direction are unaffected by the deformation, namely,

$$\kappa^{(p)} = \frac{c^{(p)}}{h^{(p)}} = \frac{\lambda^{(p)}_1\sqrt{\mu^{(p)}/\rho^{(p)}_0}}{\lambda^{(p)}_1 H^{(p)}} = \frac{\sqrt{\mu^{(p)}/\rho^{(p)}_0}}{H^{(p)}}. \tag{36}$$

To examine how the domain of $\mathbb{D}$ is changed by the deformation, assume without loss of generality that $\rho^{(1)}\mu^{(1)} > \rho^{(2)}\mu^{(2)}$; if $\lambda^{(1)}_1 > \lambda^{(2)}_1$ (resp. $\lambda^{(1)}_1 < \lambda^{(2)}_1$), then γ is greater (resp. less) than its value before the deformation, and the area of $\mathbb{D}$ increases (resp. decreases). Together with the observation made on a and $\kappa^{(p)}$, this implies that the band-gap widths increase (resp. decrease), while the middle frequency of each band-gap is unchanged.

Gentian layers are governed by Gent (1996)

$$\Psi^{(p)}\left(\mathbf{F}\right) = \frac{\mu^{(p)}J^{(p)}_m}{2}\ln\left(1 - \frac{\operatorname{tr}\mathbf{F}^{\mathrm{T}}\mathbf{F} - 3}{J^{(p)}_m}\right) - \mu^{(p)}\ln\det\mathbf{F} + \frac{\lambda^{(p)}}{2}(\ln\det\mathbf{F})^2, \tag{37}$$

for which

$$C^{(p)}_{2121} = \frac{{\lambda^{(p)}_1}^2\mu^{(p)}}{1 - \dfrac{{\lambda^{(p)}_1}^2 + \lambda_2^2 + \lambda_3^2 - 3}{J^{(p)}_m}}\Big/\lambda^{(p)}_1\lambda_2\lambda_3. \tag{38}$$

The dimensionless parameter $J_m \in (0, \infty]$ models the rapid stiffening in elastomers when approaching a limiting strain. Assume first that $J^{(1)}_m = J^{(2)}_m =: J_m$. Also assume that $\lambda^{(1)}_1 = \lambda^{(2)}_1 =: \lambda_1$, *e.g.*, when the layers are incompressible. In this case, the deformation does not modify the impedance contrast γ, and hence the gap domain $\mathbb{D}$ remains unchanged. The deformation also preserves the flow direction a_f, however it modifies the flow rate, $\mathrm{d}\vec{\zeta}/\mathrm{d}\omega$, which is multiplied by $1 - (\lambda_1^2 + \lambda_2^2 + \lambda_3^2 - 3)/J_m$. Consequently, the pertinent frequencies are multiplied by the inverse of this factor. This factor is a monotonically decreasing function of $\operatorname{tr}\mathbf{F}^{\mathrm{T}}\mathbf{F}$ with a range $(0, 1]$, as the limiting strain modeled by J_m reflects $\lambda_1^2 + \lambda_2^2 + \lambda_3^2 - 3 < J_m$. Therefore, the frequency spectrum is shifted towards higher frequencies, and its gaps are rendered wider by that factor. When $J^{(1)}_m \neq J^{(2)}_m$ or $\lambda^{(1)} \neq \lambda^{(2)}$, the flow direction changes with the deformation, and so does the impedance contrast. Thus, the spectrum is rendered tunable in a more intricate manner. The exploration of the specific way it takes effect depending on the relation between $J^{(p)}_m$ and $\lambda^{(p)}_i$, $i = 1..3$, is beyond our scope. We note, however, that following the way the aforementioned relations enter Eq. (18), the flow lines will rotate either clockwise or counter-clockwise, and the length of their intersections with the resultant domain of $\mathbb{D}$ will accordingly change. The analysis of the resultant $\Delta\omega$ is rendered simpler, by virtue of the torus universality, as for each γ, the relation between $\Delta\zeta$ and a_f is unchanged. Therefore, one can calculate the corresponding slope a_f in terms of $J^{(p)}_m$ and $\lambda^{(p)}_i$, $i = 1..3$, and employ a fixed calculation of $\Delta\zeta/\sqrt{1 + a_f^2}$, to evaluate Eq. (20).

There are additional soft systems for which "small on large" waves are described by Eq. (11); Shmuel and deBotton (2012) have derived a dispersion relation with the same functional form when analyzing the thickness vibrations of finitely deformed *dielectric elastomers*. These materials undergo finite strains and change their physical properties by application of electric stimuli (Pelrine et al., 2000; Zhao and Suo, 2010). Hence, the torus representation holds in this case as well, and

subsequently, the validity of our previous observations is established. In particular, our representation provides a platform for an investigation of the electric field effect on the spectrum.

We argue that under the similar setting to those considered by Shmuel and deBotton (2012), *magnetorehological elastomers* (Ginder et al., 1999) admit the same dispersion relation. These materials consist of ferromagnetic particles embedded in a rubber-like matrix. Application of magnetic stimuli induces magnetic forces and moments on the inclusions. This changes the microstructure of the material, and, in turn, alters its configuration and stiffness. When the particles are disturbed in a chain-like manner, the material admits a laminated structure (Galipeau and Ponte Castañeda, 2013; Rudykh and Bertoldi, 2013). We argue that our analysis also applies to these materials, in light of the similarly with soft dielectrics. First, note that under a quasi-magneto/electrostatic approximation, the governing electric and magnetic fields are differentially similar – the magnetic induction and the electric displacement fields are divergence-free, the magnetic and the electric fields are curl-free. Second, the mechanical response of both materials is governed by an elastomeric substance. The only difference is the relation between the magnetic load and the resultant stretch, on account of a different magnetic constitutive behavior. Therefore, under similar settings, the propagation of superposed waves is governed by the same dispersion relation. The applicability of our analysis thereby follows.

6. Concluding remarks

We complete this paper with a summary of our main conclusions, and a glance towards future challenges. We found that the frequency spectrum of periodic laminates admits a universal structure, independent of the geometry of their unit-cell and specific physical properties. This structure is a two-dimensional torus on which a linear flow is defined. This enabled us to derive universal properties of the spectrum, and rigorously determine the density of the band-gaps, their expected and maximal widths, and relate these to particular compositions. Thus far, the quantities above were either unknown, or determined in an approximate manner. We showed that our conclusions successfully apply to various finitely deformed materials, of tunable spectrum. We utilized our framework to characterize this tunability.

Our future objective is to extend this approach to analyze interesting generalizations of the considered systems. One such generalization is a laminate consisting of N-constituents (Lekner, 1994). Its dispersion relation is a sum of products of functions, whose arguments are $\omega h^{(p)}/c^{(p)}$, $p = 1..N$ (Shen and Cao, 2000). By change of variables in the form of Eq. (13), we can write η as a function which is 2π-periodic in N variables. Thus, a universal structure over a N-dimensional torus is obtained, and we establish a platform for analysis of N-component laminates. Materials which are periodic in more than one direction are also of interest. In these composites, a closed-form expression for the dispersion relation is not available, and series-type solutions are sought (Kushwaha et al., 1993; Vasseur et al., 2008). It is an imperative challenge to establish counterparts of the results reported herein for such materials.

Acknowledgments

G.S. acknowledges ISF (Grant no. 1912/15), BSF (Grant no. 2014358) supports. R.B. was supported by ISF (Grant no. 494/14), Marie Curie Actions (Grant no. PCIG13-GA-2013-618468) and the Taub Foundation (Taub Fellow).

Appendix A. Supplementary material

Supplementary data associated with this paper can be found in the online version at http://dx.doi.org/10.1016/j.jmps.2016.04.001.

References

Adams, Samuel D.M., Craster, Richard V., Guenneau, Sebastien, 2008. Bloch waves in periodic multi-layered acoustic waveguides. Proc. R. Soc. Lond. A: Math. Phys. Eng. Sci. 464 (2098), 2669–2692.

Band, Ram, Berkolaiko, Gregory, 2013. Universality of the momentum band density of periodic networks. Phys. Rev. Lett. 111, 130404, http://dx.doi.org/10.1103/PhysRevLett.111.130404. URL http://link.aps.org/doi/10.1103/PhysRevLett.111.130404.

Barra, F., Gaspard, P., 2000. On the level spacing distribution in quantum graphs. J. Stat. Phys. 101 (1–2), 283–319, http://dx.doi.org/10.1023/A:1026495012522.

Berkolaiko, G., Winn, B., 2010. Relationship between scattering matrix and spectrum of quantum graphs. Trans. Am. Math. Soc. 362 (12), 6261–6277, http://dx.doi.org/10.1090/S0002-9947-2010-04897-4.

Colquitt, D.J., Brun, M., Gei, M., Movchan, A.B., Movchan, N.V., Jones, I.S., 2014. Transformation elastodynamics and cloaking for flexural waves. J. Mech. Phys. Solids 72, 131–143, http://dx.doi.org/10.1016/j.jmps.2014.07.014. ISSN 0022-5096. URL ⟨http://www.sciencedirect.com/science/article/pii/S0022509614001586⟩.

deBotton, G., 2005. Transversely isotropic sequentially laminated composites in finite elasticity. J. Mech. Phys. Solids 53, 1334–1361, http://dx.doi.org/10.1016/j.jmps.2005.01.006.

Destrade, M., Saccomandi, G. (Eds.), 2007. Waves in Nonlinear Pre-stressed Materials. CISM Course and Lectures. Springer, Wien, NY.

Elser, D., Andersen, U.L., Korn, A., Glöckl, O., Lorenz, S., Marquardt, Ch., Leuchs, G., 2006. Reduction of guided acoustic wave brillouin scattering in photonic crystal fibers. Phys. Rev. Lett. 97 (September), 133901, http://dx.doi.org/10.1103/PhysRevLett.97.133901. URL http://link.aps.org/doi/10.1103/PhysRevLett.97.133901.

Farzbod, Farhad, Leamy, Michael J., 2011. Analysis of Bloch's method and the propagation technique in periodic structures. J. Vib. Acoust. 133 (3), 031010. URL http://dx.doi.org/10.1115/1.4003202http://dx.doi.org/10.1115/1.4003202.

Gent, A.N., 1996. A new constitutive relation for rubber. Rubber Chem. Technol. 69, 59–61.

Ginder, John M., Nichols, Mark E., Elie, Larry D., Tardiff, Janice L., 1999. Magnetorheological elastomers: properties and applications, SPIE 3675, 131-138.

Gomopoulos, N., Maschke, D., Koh, C.Y., Thomas, E.L., Tremel, W., Butt, H.-J., Fytas, G., 2010. One-dimensional hypersonic phononic crystals. Nano Lett. 10 (3), 980–984, http://dx.doi.org/10.1021/nl903959r. PMID: 20141118.

Graff, K.F., 1975. Wave Motion in Elastic Solids. Dover Books on Physics Series. Dover Publications ISBN 9780486667454. URL ⟨https://books.google.co.il/books?id=5cZFRwLuhdQC⟩.

Henderson, B.K., Maslov, K.I., Kinra, V.K., 2001. Experimental investigation of acoustic band structures in tetragonal periodic particulate composite structures. J. Mech. Phys. Solids 49 (10), 2369–2383, http://dx.doi.org/10.1016/S0022-5096(01)00019-9. ISSN 0022-5096.

Katok, A., Hasselblatt, B., 1996. Introduction to the Modern Theory of Dynamical Systems. Cambridge University Press. (1997, Ohio State University Press).

Khelif, A., Choujaa, A., Djafari-Rouhani, B., Wilm, M., Ballandras, S., Laude, V., 2003. Trapping and guiding of acoustic waves by defect modes in a full-band-gap ultrasonic crystal. Phys. Rev. B 68 (December), 214301, http://dx.doi.org/10.1103/PhysRevB.68.214301. URL http://link.aps.org/doi/10.1103/PhysRevB.68.214301.

Kim, Eunho, Yang, Jinkyu, 2014. Wave propagation in single column woodpile phononic crystals: formation of tunable band gaps. J. Mech. Phys. Solids 71, 33–45, http://dx.doi.org/10.1016/j.jmps.2014.06.012. ISSN 0022-5096. URL ⟨http://www.sciencedirect.com/science/article/pii/S0022509614001380⟩.

Kushwaha, M.S., Halevi, P., Dobrzynski, L., Djafari-Rouhani, B., 1993. Acoustic band structure of periodic elastic composites. Phys. Rev. Lett. 71 (13), 2022–2025.

Lekner, John, 1994. Light in periodically stratified media. J. Opt. Soc. Am. A 11 (November (11)), 2892–2899, http://dx.doi.org/10.1364/JOSAA.11.002892. URL ⟨http://josaa.osa.org/abstract.cfm?URI=josaa-11-11-2892⟩.

Milton, Graeme W., Briane, Marc, Willis, John R., 2006. On cloaking for elasticity and physical equations with a transformation invariant form. New J. Phys. 8 (10), 248. URL ⟨http://stacks.iop.org/1367-2630/8/i=10/a=248⟩.

Miyashita, Toyokatsu, 2005. Sonic crystals and sonic wave-guides. Meas. Sci. Technol. 16 (5), R47. URL ⟨http://stacks.iop.org/0957-0233/16/i=5/a=R01⟩.

Mullin, T., Deschanel, S., Bertoldi, K., Boyce, M.C., 2007. Pattern transformation triggered by deformation. Phys. Rev. Lett. 99, 084301.

Nemat-Nasser, Sia, Srivastava, Ankit, 2011. Overall dynamic constitutive relations of layered elastic composites. J. Mech. Phys. Solids 59 (10), 1953–1965, http://dx.doi.org/10.1016/j.jmps.2011.07.008. ISSN 0022-5096. URL ⟨http://www.sciencedirect.com/science/article/pii/S0022509611001475⟩.

Ogden, R.W., 1997. Non-Linear Elastic Deformations. Dover Publications, New York.

Olsson III, R.H., El-Kady, I., 2009. Microfabricated phononic crystal devices and applications. Meas. Sci. Technol. 20 (1), 012002. URL ⟨http://stacks.iop.org/0957-0233/20/i=1/a=012002⟩.

Pelrine, R., Kornbluh, R., Pei, Q.-B., Joseph, J., 2000. High-speed electrically actuated elastomers with strain greater than 100%. Science 287, 836–839.

Psarobas, I.E., Papanikolaou, N., Stefanou, N., Djafari-Rouhani, B., Bonello, B., Laude, V., 2010. Enhanced acousto-optic interactions in a one-dimensional phoxonic cavity. Phys. Rev. B 82 (November), 174303, http://dx.doi.org/10.1103/PhysRevB.82.174303. URL http://link.aps.org/doi/10.1103/PhysRevB.82.174303.

Qian, Zhenghua, Jin, Feng, Wang, Zikun, Kishimoto, Kikuo, 2004. Dispersion relations for sh-wave propagation in periodic piezoelectric composite layered structures. Int. J. Eng. Sci. 42 (7), 673–689, http://dx.doi.org/10.1016/j.ijengsci.2003.09.010. ISSN 0020-7225. URL ⟨http://www.sciencedirect.com/science/article/pii/S002072250400014X⟩.

Robertson, Jaimee M., Torbati, Amir H., Rodriguez, Erika D., Mao, Yiqi, Baker, Richard M., Jerry Qi, H., Mather, Patrick T., 2015. Mechanically programmed shape change in laminated elastomeric composites. Soft Matter 11, 5754–5764, http://dx.doi.org/10.1039/C5SM01004G.

Rudykh, Stephan, Bertoldi, Katia, 2013. Stability of anisotropic magnetorheological elastomers in finite deformations: a micromechanical approach. J. Mech. Phys. Solids 61 (4), 949–967.

Rudykh, Stephan, Boyce, Mary C., 2014. Transforming wave propagation in layered media via instability-induced interfacial wrinkling. Phys. Rev. Lett. 112 (January), 034301, http://dx.doi.org/10.1103/PhysRevLett.112.034301. URL http://link.aps.org/doi/10.1103/PhysRevLett.112.034301⟩.

Ruzzene, M., Baz, A., 1999. Control of wave propagation in periodic composite rods using shape memory inserts. J. Vib. Acoust. 122 (June (2)), 151–159. URL http://dx.doi.org/10.1115/1.568452http://dx.doi.org/10.1115/1.568452.

Shen, Mingrong, Cao, Wenwu, 2000. Acoustic bandgap formation in a periodic structure with multilayer unit cells. J. Phys. D: Appl. Phys. 33 (10), 1150. URL ⟨http://stacks.iop.org/0022-3727/33/i=10/a=303⟩.

Shmuel, G., deBotton, G., 2012. Band-gaps in electrostatically controlled dielectric laminates subjected to incremental shear motions. J. Mech. Phys. Solids 60, 1970–1981.

Shmuel, Gal, Band, Ram, 2016. Spectral statistics of layered photonic crystals are universal, in preparation.

Smith, W.A., Auld, B.A., 1991. Modeling 1–3 composite piezoelectrics: thickness-mode oscillations. IEEE Trans. Ultrason. Ferroelectr. Freq. Control 38 (January (1)), 40–47, http://dx.doi.org/10.1109/58.67833. ISSN 0885-3010.

Vasseur, J.O., Deymier, P.A., Djafari-Rouhani, B., Pennec, Y., Hladky-Hennion, A.-C., 2008. Absolute forbidden bands and waveguiding in two-dimensional phononic crystal plates. Phys. Rev. B 77, 085415.

Walker, P.M., Sharp, J.S., Akimov, A.V., Kent, A.J., 2010. Coherent elastic waves in a one-dimensional polymer hypersonic crystal. Appl. Phys. Lett. 97 (7), 073106, http://dx.doi.org/10.1063/1.3479929. URL ⟨http://scitation.aip.org/content/aip/journal/apl/97/7/10.1063/1.3479929⟩.

Wang, Pai, Casadei, Filippo, Shan, Sicong, Weaver, James C., Bertoldi, Katia, 2014. Harnessing buckling to design tunable locally resonant acoustic metamaterials. Phys. Rev. Lett. 113, 014301.

Willis, J.R., 2009. Exact effective relations for dynamics of a laminated body. Mech. Mater. 41 (4), 385–393, http://dx.doi.org/10.1016/j.mechmat.2009.01.010. ISSN 0167-6636. URL ⟨http://www.sciencedirect.com/science/article/pii/S0167663609000118⟩. (The Special Issue in Honor of Graeme W. Milton).

Yablonovitch, E., 1993. Photonic band-gap crystals. J. Phys.: Condens. Matter 5, 2443–2460.

Zhao, Xuanhe, Suo, Zhigang, 2010. Theory of dielectric elastomers capable of giant deformation of actuation. Phys. Rev. Lett. 104 (April), 178302, http://dx.doi.org/10.1103/PhysRevLett.104.178302. URL http://link.aps.org/doi/10.1103/PhysRevLett.104.178302.

Ziegler, F., 1977. Wave propagation in periodic and disordered layered composite elastic materials. Int. J. Solids Struct. 13, 293–305.